Phase transitions in Zr to 240 GPa

J. D. McHardy,* C. V. Storm, C. M. Lonsdale, C. R. Roy, and M. I. McMahon†
SUPA, School of Physics and Astronomy, and Centre for Science at Extreme Conditions, The University of Edinburgh, Peter Guthrie Tait Road, Edinburgh EH9 3FD, United Kingdom

(Received 19 January 2026; revised 22 April 2026; accepted 29 April 2026; published 18 May 2026)

Several recent x-ray diffraction studies have focused on whether the high-pressure body-centered cubic (bcc) phase of zirconium undergoes an isostructural bcc-bcc transition at 58 GPa. The consensus of these studies is that there is no such transition and that a previous claim by Stavrou *et al.* resulted from issues with the pressure calibration. However, a close analysis of the data from one of the most recent of these diffraction studies by Anzellini *et al.* shows unremarked evidence of a discontinuity in both atomic volume and compressibility at 83 GPa indicating an isostructural transition is present. Unfortunately, no other previous studies have reached this pressure, and so the question of the bcc-bcc transition is still open. Here we describe a diffraction study of Zr to 240 GPa looking for a bcc-bcc isostructural transition. Our data show no evidence of any discontinuous change in volume or compressibility at 83 GPa. We observe no evidence of a $\beta \rightarrow \beta'$ transition above 80 GPa, and suggest a possible cause of the discontinuity observed by Anzellini *et al.*

DOI: 10.1103/zp3m-kjpc

I. INTRODUCTION

The group IVb elements, Ti, Zr, and Hf, and their alloys, have physical properties, such as high strength-to-weight ratio, excellent mechanical properties, and corrosion resistance, ideally suited to their use under extreme conditions. Their performance can be improved further by manipulating the crystallographic forms present and optimizing their microstructure [1,2]. Such material design requires an accurate knowledge of their phase diagrams [3], and so studies under extreme conditions have been frequent and remain ongoing. Ti, Zr, and Hf each crystallize in the hexagonal close-packed (hcp, or $hP2$ in Pearson notation) crystal structure at ambient conditions, also known as the α phase. On compression, all three elements transform to the brittle ω phase ($hP3$ in Pearson notation) at only modest pressures, the presence of which in alloys greatly affects their toughness and ductility [1,4]. Further compression in Ti results in structural transitions to two orthorhombic phases before a final transition to a body-centered cubic structure (bcc, β-Ti, or $cI2$) at ∼240 GPa [5]. In contrast, Zr transforms directly to bcc β-Zr from ω-Zr at only 30–35 GPa [6], and earlier claims of a rare isostructural bcc → bcc phase transition at 58 GPa [7,8] have since been questioned [9–11].

This isostructural transition in Zr is the focus of this study. Before describing the results, however, we provide a short summary of previous high-pressure diffraction and computational studies of Zr, highlighting the differences between them.

Previous diffraction and computational investigations of Zr

The bcc phase of Zr (β-Zr) was first reported by Xia *et al.* [6] in 1990, who studied Zr up to 32 GPa using energy-dispersive powder diffraction, and reported the $\omega \rightarrow \beta$ transition to occur between 31.1 and 31.6 GPa. Soon afterwards, Akahama *et al.* [7], in one of the first studies using angle-dispersive diffraction techniques and 2D image plate detectors, pushed the upper pressure limit to 68 GPa, and reported that they saw the transition to β-Zr at 33 GPa, with a further first-order bcc → bcc ($\beta \rightarrow \beta'$) transition at ∼56 GPa, coupled to a volume change of 1.2%. The possible existence of an isostructural transition in Zr prompted two computational studies of the Zr equation of state, to 126 GPa by Jyoti and Gupta [12] and to 80 GPa by Greeff [13]. In neither study was a discontinuity observed in the calculated compressibility of β-Zr that would indicate an isostructural $\beta \rightarrow \beta'$ transition.

Surprisingly, there were then no further diffraction studies of Zr until 2018, when Stavrou *et al.* [8], using a sample loaded without a pressure transmitting medium (PTM), greatly extended the upper pressure limit to 210 GPa. These authors also reported a $\beta \rightarrow \beta'$ transition, at 58 GPa, with a clear volume change of 4%. The experimental results were backed by first-principles quantum molecular dynamics calculations, which supported the existence of the isostructural transition triggered by anharmonic motion [8].

The possible existence of a pressure-induced isostructural transition in Zr—seen otherwise only in Ce [14,15] among the elements—has prompted a number of further studies, focused on this transition. Pigott *et al.* [9] studied Zr to 70 GPa in a He PTM, and to 74 GPa without a PTM. In neither sample was

*Contact author: J.D.McHardy@ed.ac.uk
†Contact author: m.i.mcmahon@ed.ac.uk

Published by the American Physical Society under the terms of the Creative Commons Attribution 4.0 International license. Further distribution of this work must maintain attribution to the author(s) and the published article's title, journal citation, and DOI.

the $\beta \rightarrow \beta'$ transition observed. Further studies by Anzellini *et al.* [10] to 142 GPa using four samples in He and Ne PTMs, and by O'Bannon *et al.* [11], using three samples compressed in a Ne PTM, also reported no isostructural $\beta \rightarrow \beta'$ transition. As a result, Pigott *et al.*, Anzellini *et al.*, and O'Bannon *et al.* concluded that the results of Stavrou *et al.* arose from a pressure difference between the sample and the pressure marker. The studies of Anzellini *et al.* [10] and O'Bannon *et al.* [11] also included computational results, neither of which showed any evidence of a $\beta \rightarrow \beta'$ transition, and Anzellini *et al.* concluded that the volume change reported by Stavrou *et al.* arose from their use of insufficient k points in their molecular dynamics calculations.

Finally, in the most recent 2023 study, Liu *et al.* [16] used a high-purity sample loaded in an Ar PTM, and studied β-Zr to 68 GPa. Their compression data were in reasonable agreement with those obtained by Pigott, Anzellini, and O'Bannon, and they also saw no evidence of the $\beta \rightarrow \beta'$ transition. They concluded that this transition does not exist, or that if it does exist, then it takes place at a higher pressure than has been reached in any of the studies to date.

In this regard, it is notable that, with the exception of Anzellini *et al.*, no recent study of β-Zr using a PTM has exceeded a pressure of 80 GPa. This is unfortunate, as close inspection of the compression data obtained in Run4 (R4) by Anzellini *et al.* (see Fig. 5 of Ref. [10]) shows a small discontinuity in both volume (0.2%) and compressibility at 83 GPa, as identified by the arrow in Fig. 1(a) and its inset. While the discontinuities in volume and bulk modulus are perhaps difficult to see in the raw P-V data of Fig. 1(a), we have recently demonstrated that such changes are more readily observed in linearized compressibility plots [17,18], particularly the linearization scheme based on Holzapfel's Adapted Polynomial of order L (APL) EoS formalism [19,20].

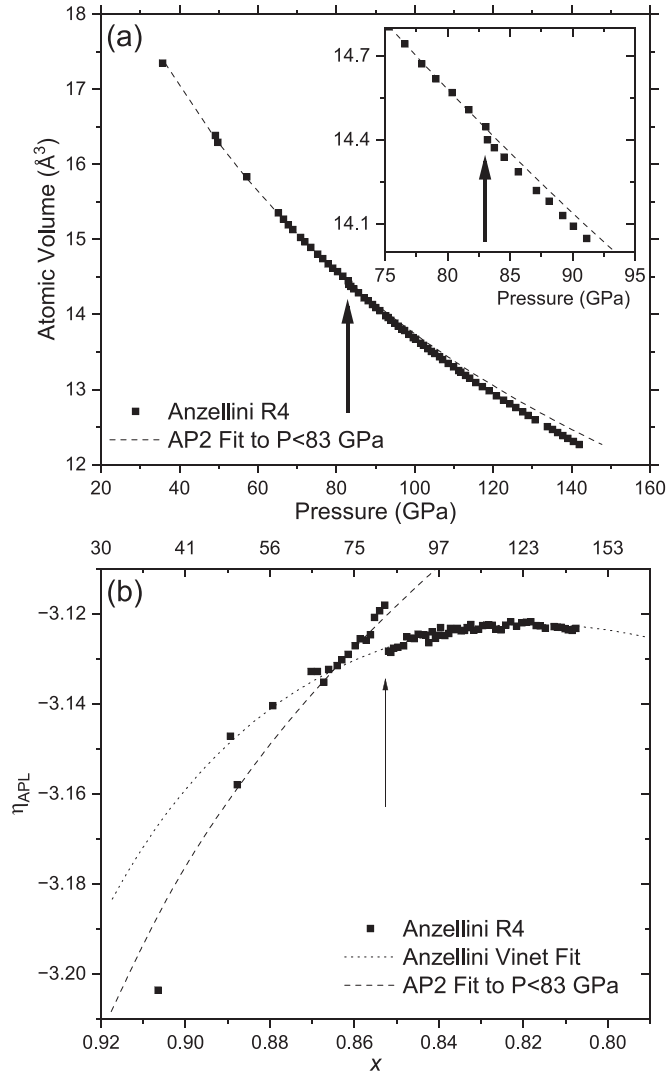


FIG. 1. (a) The volume compressibility of bcc-Zr to 142 GPa, as determined in Run4 (R4) of the recent study of Anzellini *et al.* [10]. The data were extracted from Fig. 5 of Ref. [10] using WebPlotDigitizer 4.5 [21]. There is a small, but distinct, discontinuity in both volume and compressibility in the P-V data at 83 GPa, as highlighted by the arrows in the main panel and the enlarged inset. The dashed line shows the AP2 equation of state fitted to those data collected below 83 GPa. (b) The discontinuity (at $x = (V/V_0)^{1/3} = 0.852$) is much more evident when the data are linearized in x-η_{APL} space. The dashed line shows the linearized AP2 equations of state plotted in (a), while the dotted line shows the linearized Vinet equation of state plotted in Fig. 5 of Ref. [10].

II. APL LINEARIZATION SCHEME

We examine the previous compression data of Anzellini *et al.* in the context of the APL EoS formalism:

$$P(x) = 3K_0 \frac{(1-x)}{x^5} e^{c_0(1-x)} \left[1 + x \sum_{k=2}^{L} c_k (1-x)^{k-1} \right], \quad (1)$$

where P is the pressure as a function of x, K_0 is the zero-pressure bulk modulus, K_0' is its pressure derivative, $x = (V/V_0)^{1/3}$, $c_0 = -\ln(3K_0/P_{FG0})$, $c_2 = (3/2)(K_0' - 3) - c_0$, and c_k are independent fitting parameters for $k \in [3, ..., L]$, $P_{FG0} = a_{FG0}(Z/V_0)^{(5/3)}$ is the Fermi-gas pressure, Z is the atomic number, and $a_{FG0} = 2337$ GPa Å^5 is a constant. Note that in the lowest-order AP1 ($L = 1$) case, the summation term is zero and the only refinable parameters are the ambient volume (V_0) and bulk modulus (K_0), with K_0' being calculated from $K_0' = 3 + (2/3)c_0$.

Changes in the compression behavior is clearer when the experimental data are displayed in the so-called $x - \eta_{APL}$ plot which, as stated, provides a linearized space for the APL formalism. With $L = 1$, the linearization gives

$$\eta_{APL}(x) = \ln\left(\frac{Px^5}{P_{FG0}(1-x)}\right), \quad (2)$$

with variables and constants as in Eq. (1). Thus, in the APL formalism, "simple" metals are well described by a first-order AP1 EoS and exhibit linear behavior with

$$\lim_{x \to 1} \eta_{APL}(x) = \ln\left(\frac{3K_0}{P_{FG0}}\right), \quad (3)$$

and

$$\lim_{x \to 0} \eta_{APL}(x) = 0, \quad (4)$$

often with a gradient ($\mathrm{d}\eta/\mathrm{d}x$) close to the "ideal" value of $\beta_{\text{ideal}} = 0.567$ Å^{-1} determined through a comparison of the

ambient pressure data across many "regular" elements [22]. Materials may be considered "regular" when instead they are well fitted by a second-order AP2 ($L = 2$) EoS following a quasilinear trend, with small c_2 parameter, extrapolating towards the origin of the linearized plot [23].

Linearization of Anzellini data

An AP2 fit we made to the R4 Anzellini data (collected from β-Zr below 83 GPa) is shown by the dashed line in Fig. 1(a), and shows that the data and the fit clearly diverge above 83 GPa. Figure 1(b) shows the same R4 Anzellini data in the APL linearized space, along with their published Vinet EoS, and the AP2 EoS we fitted to only data below 83 GPa [the same AP2 fit graphed in Fig. 1(a)]. While the compressibility of β-Zr below 83 GPa follows a quasilinear path, there is a very clear discontinuity in the compressibility at 83 GPa, such that above that pressure the compressibility of β-Zr is higher than one would expect from the data obtained below 83 GPa. Although less exaggerated, the increase in compressibility is also evident in Fig. 1(a), which shows deviation of the AP2 EoS from the R4 data when extrapolated to 150 GPa. The divergence in the data above 83 GPa is clear. We have also linearized the same R4 Anzellini data using linearization spaces applicable to the Vinet and Birch-Murnaghan EoS formalisms illustrating the discontinuity is also evident in these spaces. A comparison to the APL linearization is given in Fig. S3 of the Supplemental Material [24].

There *is* then evidence of a subtle isostructural $\beta \rightarrow \beta'$ transition in the R4 compression data of Anzellini at 83 GPa, but *only* in these data, as no other recent study has compressed β-Zr to above 80 GPa. To investigate this effect further, we have therefore collected room temperature diffraction data from Zr to 240 GPa to determine its higher pressure structural evolution. We observe no evidence of a $\beta \rightarrow \beta'$ transition above 80 GPa, and suggest a possible cause of the discontinuity observed by Anzellini *et al.*

III. EXPERIMENTAL DETAILS

A. X-ray diffraction measurements

Samples of Zr foil (purity 99.7%), supplied by Goodfellow metals, were loaded into four Boehler-Almax plate diamond-anvil cells (DACs 1, 2, 3, and 4) [25], and one membrane-driven DAC (DAC5). Each DAC was equipped with a tungsten (W) or rhenium (Re, DAC2) gasket and diamonds [26] beveled to culet diameters of 100 μm (DAC1) and 40 μm (DAC2), or nonbeveled diamonds with a diameter of 300 μm (DACs 3, 4, and 5). The sample in DAC1 was loaded fully encased within a Bi PTM, which we have recently shown can produce quasihydrostatic conditions to 298 GPa [27]. The sample chamber in DAC2 was too small to include sufficient Bi to fully encase the Zr sample, but sufficient Bi was added to be used as a pressure calibrant. The samples in DAC3, DAC4, and DAC5 were loaded fully encased within an Al PTM, which provides quasihydrostatic conditions to moderate pressures [28], and the diffraction peaks from which, unlike those from the phases of Bi-I and Bi-II at low pressures, do not overlap with those from α-Zr and ω-Zr. A summary table of the different DAC configurations is given in Table S1 in the Supplemental Material [24].

Diffraction data were collected during two beamtimes on the Extreme Conditions P02.2 beamline at the PETRA III synchrotron in Hamburg, Germany. In both cases, the monochromatic x-ray beam had a wavelength of 0.4851 Å, and was focused down to a full-width at half-maximum (FWHM) of 850 nm × 850 nm [29]. The powder-diffraction data were recorded on a Perkin-Elmer area detector, placed ∼ 330 mm from the sample. A CeO_2 diffraction standard was used to calibrate the exact sample-detector distance and the detector tilt.

The two-dimensional (2D) diffraction images collected at each pressure were integrated azimuthally using Dioptas [30] to obtain standard one-dimensional diffraction profiles, which were then analyzed using Le Bail profile-fitting methods in Jana2006 [31] or by least-squares fitting to the measured d spacings of individual diffraction peaks [32]. Parasitic diamond reflections, such as those highlighted in Figs. 2(a)–2(c), were masked on a per image basis prior to azimuthal integration. During integration, a polarization correction was applied in Dioptas to the intensities. Using standard Dioptas tools, a Chebychev polynomial function was fitted to the background of the integrated 1D profiles and subtracted. Lattice parameter uncertainties were exported from the Jana LeBail refinements of the integrated profiles and incorporated Berer's factor, or were evaluated from the standard error on the mean after fitting individual reflections with PseudoVoigt functions. Preferred orientation, anisotropic peak broadening or strain broadening modeling were not included in the LeBail fits. Pressure was determined from the embedded standards using either the AP2 Bi EoS of Storm *et al.* [27] or the Vinet Al EoS of Dewaele *et al.* [33] depending on the sample configuration. The EoS parameters used are listed in Table S4 in the Supplemental Material [24]. The 2D diffraction images and background-subtracted integrated profiles from β-Zr at 156 GPa in DAC1, 241 GPa in DAC2 (the highest pressures reached with each sample), and from ω-Zr at 32 GPa in DAC4, are shown in Fig. 2.

Although the focus of this paper is on β-Zr, for completeness, DACs 3, 4, and 5 were used to obtain compression data from α-Zr, ω-Zr, and β-Zr at lower (< 50 GPa) pressures including decompression data on the metastable ω-Zr phase to ambient pressure. At each pressure in DAC2, diffraction data were typically collected at two locations within the sample chamber, one where diffraction peaks from the Bi pressure marker were clearly visible and balanced in intensity with the Zr, and the second where the diffraction signal from the Zr was maximized. This was possible even in a sample chamber ∼10 μm in diameter due to the tight focusing of the x-rays. In addition, the submicron beam available on beamline P02.2 enabled us to map the pressure distribution in each sample every ∼25 GPa using grid scans. Representative results at a central pressure of ∼130 GPa, the highest pressure at which a grid scan of the entire gasket hole was made on DAC1, are shown in Fig. S1 in the Supplemental Material [24]. Notably, the FWHM of the x-ray beam is small in comparison to the pressure gradients present over the sample chamber, negating their effect on the collected diffraction data.

The compressibility data presented in Fig. 3 were obtained from those diffraction profiles where diffraction peaks from both Zr and Bi/Al were visible (see

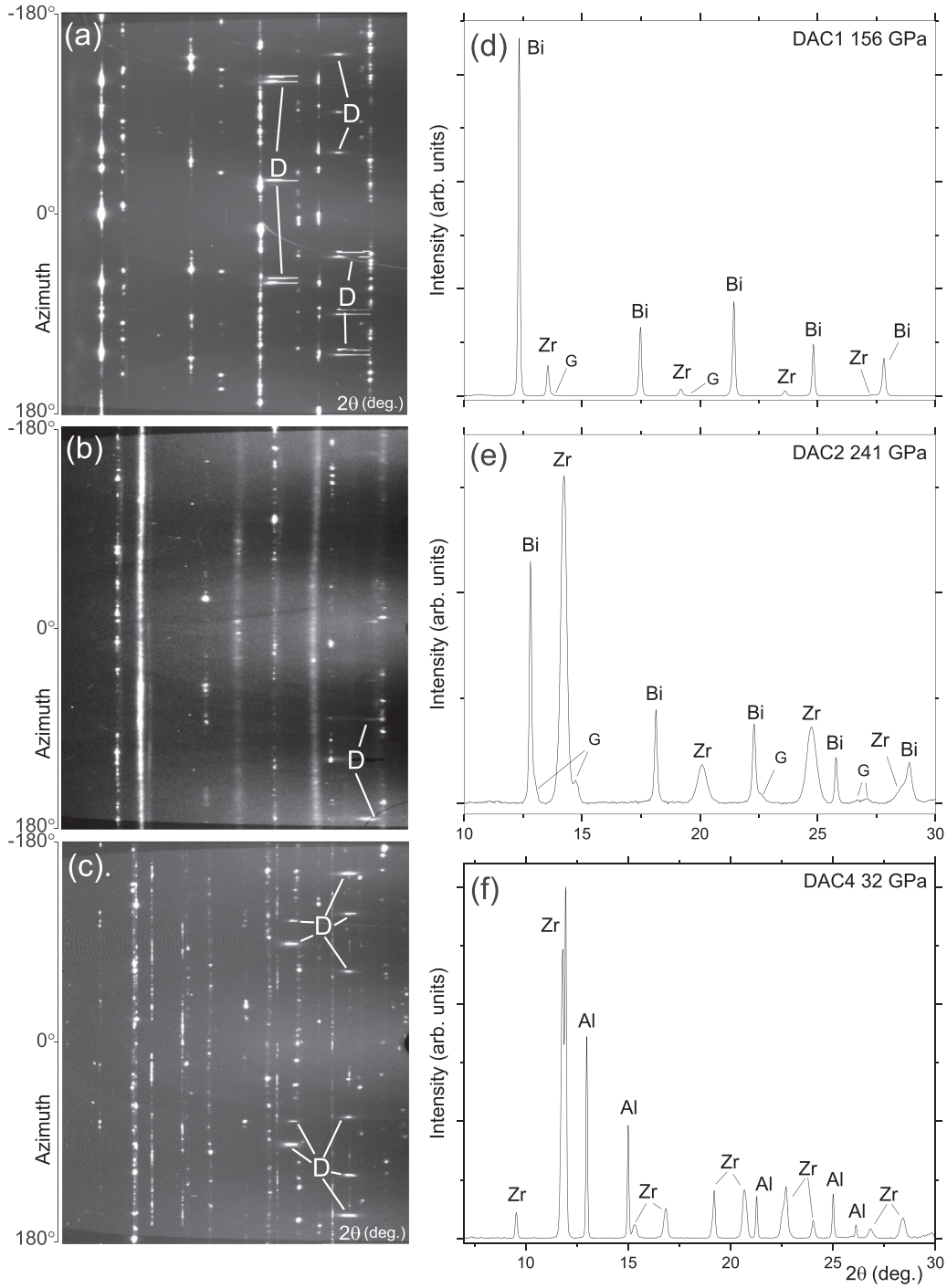


FIG. 2. The 2D Debye-Scherrer (DS) diffraction images collected from (a) β-Zr in DAC1 at 156 GPa, (b) β-Zr in DAC2 at 241 GPa, the highest pressures reached within each sample, and (c) ω-Zr in DAC4 at 32 GPa using an Al PTM. The images are presented as 2θ-azimuth angle 'cake' plots where the circular DS rings become vertical lines of constant 2θ. Diffraction features arising from the diamond anvils are labeled with 'D'. The resulting background-subtracted integrated profiles are shown in (d)–(f), with the peaks from the Zr sample and the Bi and Al PTMs, identified. The profile in (e) contains two weak diffraction peaks from the rhenium gasket, which are labeled with 'G'.

Fig. 2), so that the local pressure could be measured precisely.

B. Sample local stress state

To determine the hydrostaticity in DACs 1 and 2, which reached the highest pressures, we performed a standard analysis to evaluate the uniaxial stress component, t, in both the Zr and Bi as a function of pressure [34–36]. Here, $t = (\sigma_{33} - \sigma_{11})$, and σ_{33} and σ_{11} are the axial and radial stress components, respectively, acting on the sample [34,37]. The effect of a nonzero t is to systematically offset the diffraction peaks from the positions calculated from the hydrostatic cubic lattice parameter. The shift in position is dependent on the

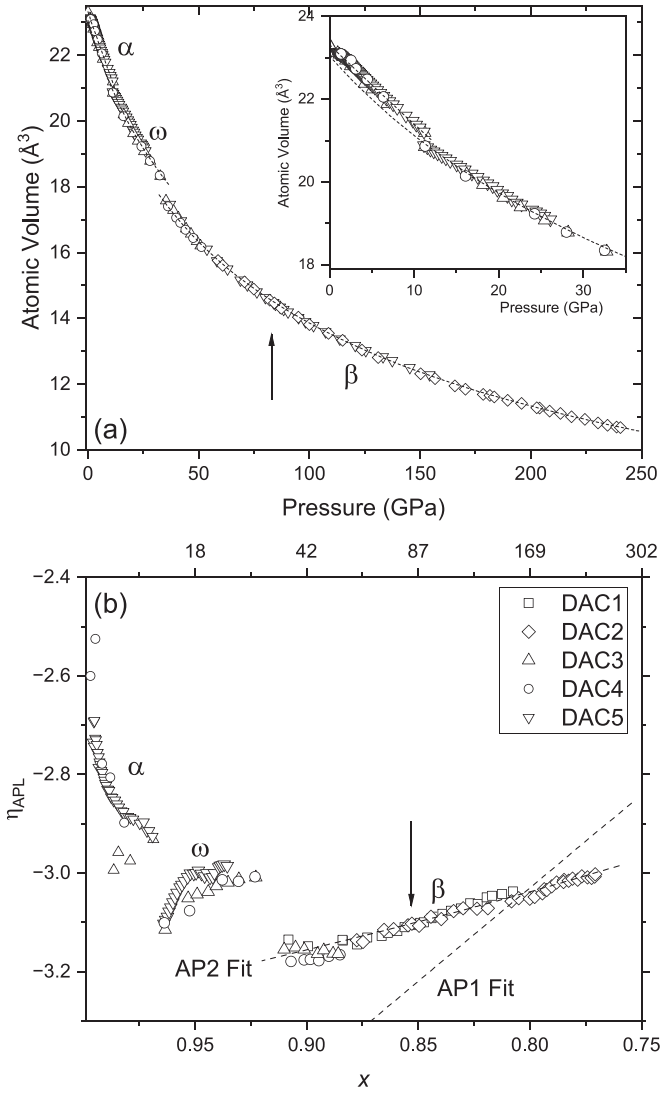


FIG. 3. (a) The volume compressibility of the α, ω, and β phases of Zr to 241 GPa. The data from the five different samples are plotted using different symbols. The dashed lines show the best-fitting AP2 EoS fits to each of the three phases. Error bars on the data are smaller than the plotting symbols and have therefore been omitted. (b) The same compression data shown as a linearized x-η_{APL} plot, along with linearized AP1 and AP2 fits to the β-Zr data. The equivalent quasilogarithmic pressure scale is shown on the top axis. The arrows in (a) and (b) show the location of the discontinuity at 83 GPa present in the data of Anzellini *et al.* (see Fig. 1). Error bars have been omitted for clarity. See Supplemental Material Fig. S5 [24] for a plot including errors.

value of t and the Miller indices (hkl) associated with the individual diffraction peaks.

Through x-ray diffraction, we measure the shifted peak positions and, by extension, the stress-modified d spacings $[d_m(hkl)]$ and associated lattice parameters $[a_m(hkl)]$. These measured lattice parameters, determined from each diffraction peak, are related to the hydrostatic lattice parameter (a_p) through

$$a_m(hkl) = a_p[1 + (1 - 3\cos^2\psi)Q(hkl)], \tag{5}$$

where ψ is the angle between the applied load (compression axis) and the diffracting plane normal, and $Q(hkl)$ is comprised of a linear combination of the shear modulus in the isostress (Reuss, G_R) and isostrain (Voigt, G_V) limits

$$Q(hkl) = \frac{t}{3}\left(\alpha\left[2G_R^X(hkl)\right]^{-1} + (1-\alpha)[2G_V]^{-1}\right). \tag{6}$$

The parameter α determines the relative weights of the Reuss and Voigt models and the superscript X denotes the x-ray sampling of reflections contributing to the calculation of the Reuss shear modulus [34,35,37–39].

In conventional axial geometry, where the x-ray beam and compression axis are coaxial, ψ from Eq. (5) is equal to $\pi/2 - \theta$ (θ being the Bragg angle), such that $\cos^2\psi = \sin^2\theta$, and the shear moduli are functions of the elastic moduli C_{ij} and $\Gamma(hkl)$ where

$$\Gamma(hkl) = \frac{h^2k^2 + k^2l^2 + l^2h^2}{(h^2 + k^2 + l^2)^2}. \tag{7}$$

The relation between the shear moduli and the elastic constants is crystal structure dependent. For cubic symmetry, we have

$$[2G_V]^{-1} = 5/(2(C_{11} - C_{12} - 3C_{44})), \tag{8}$$

and

$$\left[2G_R^X(hkl)\right]^{-1} = \frac{1}{C_{11} - C_{12}} - 3S\Gamma(hkl), \tag{9}$$

where S is the elastic anisotropy parameter for a cubic system

$$S = 1/(C_{11} - C_{12}) - 1/(2C_{44}). \tag{10}$$

Thus, by making so-called Γ-plots of $a_m(hkl)$ versus $3(1 - 3\sin^2\theta)\Gamma(hkl)$, the uniaxial stress component t can be approximated from

$$t \sim -3M_1/(\alpha M_0 S), \tag{11}$$

where M_1 and M_0 are the gradient and y-axis intercept of a linear fit to the data in the Γ-plot. For comparison with the same analysis performed by O'Bannon *et al.* [11], we have used $\alpha = 1$ (i.e., Reuss isostress limit), which gives the lower bound for the value of t, and have used the values of C_{ij} calculated by the same authors to 717 GPa.

The stress analysis described assumes that σ_{33} is acting along the DAC axis, and in a standard axial diffraction geometry the Debye-Scherrer rings remain circular but have their radii changed by t. However, if σ_{33} is not coincident with the DAC axis, then the Debye-Scherrer rings will be distorted from circular and their radii change with azimuth around the ring. Such distortions are most evident in 2θ-azimuth angle "cake" plots, such as those shown in Figs. 2(a)–2(c), where they manifest as "wiggles" in the otherwise straight Debye-Scherrer lines.

Example Γ-plots for the Zr and Bi at several pressures are shown in Fig. S4 of the Supplemental Material [24], while the pressure variation of t in both the Zr and Bi is shown in Figs. 4(a) and 4(b), respectively. The values of t in the bismuth PTM are small (<1 GPa) at all pressures up to ~200 GPa, confirming it as a good pressure medium and standard as previously shown [27]. Interestingly, the values

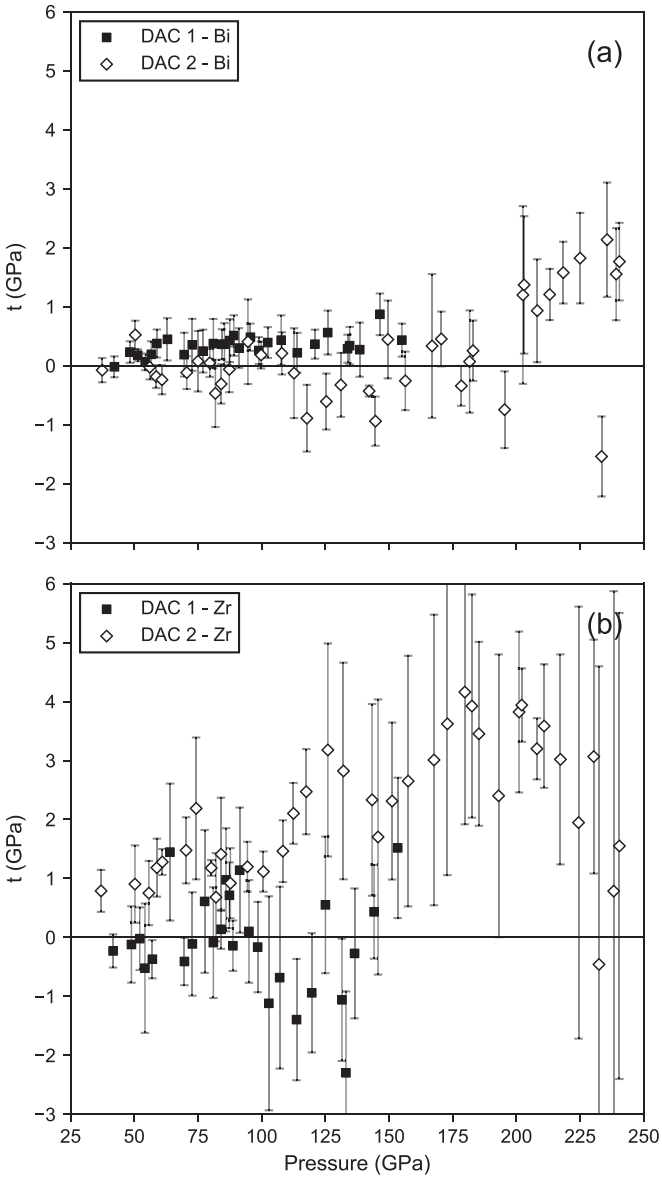


FIG. 4. The uniaxial stress component, t as a function of pressure evaluated from between 5 (Zr) to 7 (Bi) Bragg reflections for (a) Bi and (b) Zr in DACs 1 and 2. Both DACs contained beveled anvils with either 300/100 (DAC1) or 300/40 (DAC2) micron diameter culets. As such, the Zr sample in DAC1 was fully encased in the Bi medium while DAC2 only contained sufficient Bi to act as an internal standard.

of t in the Zr in DAC 1 are predominantly negative, indicating that the radial stress component of the sample (σ_{11}) is larger than the axial component (σ_{33}). Such effects are typically seen when the gasket hole containing the sample is deforming inward [40]. However, we see such effects at relatively low pressures in the Zr, and not in the Bi surrounding or adjacent to the Zr, suggesting that gasket hole deformation is not the cause of the negative t in this case. We note that values of M_1 in the Γ-plots published by Anzellini *et al.* indicate that negative values of t were also obtained in that study, while O'Bannon's analysis [11] of the Stavrou *et al.* [8] data reveals that negative values of t were also seen in that study below 60 GPa. O'Bannon *et al.* themselves reported small, but positive, values of t [11].

From Fig. 4(b), our stress analysis suggests a significant rise in the t value in Zr for DAC2 (no PTM) at pressures between $\sim 175 - 200$ GPa reaching a maximum value on the order of $t = 4$ GPa. However, we note that the t values obtained through this analysis are likely a poor representation of the actual stress state in the DACs. The analysis is highly sensitive to the inclusion or exclusion of certain reflections in the Γ-plot fits. For example, referring to the selected Zr Γ-plots in Fig. S4, we see the (103) reflection sits to the left-hand side along the x axis. Without this reflection, the plots are severely biased by the position of the (002) reflection. We have observed similar effects in other bcc metals [41]. Given that both the (002) and (103) are not particularly strong reflections, and the (103) peak intensity appears at high scattering angles ($2\theta \sim 32^\circ$) there is increased uncertainty associated in their positions. In some instances, it was not possible to determine the (103) position at all. Furthermore, with increasing pressure, the value of the anisotropy parameter, S, decreases rapidly and is particularly small above $\sim$50 GPa. This means β-Zr exhibits a relatively elastic response under deviatoric stresses making the stress analysis extremely sensitive to small variations in the slope and intercept of the Γ-plots since S appears in the denominator of Eq. (11). Additionally, some of the highest pressure patterns displayed evidence of subtle "wiggles" in the cake plots [e.g., Fig. 2(b)] which manifest when the principal stress axis is offset with the x-ray beam. This offset undermines assumptions required for the analysis approach and may lead to erroneous t values when applying this method in some instances.

To this point, we highlight the excellent agreement displayed between the DAC1 (PTM) and DAC2 (no PTM) datasets in the linearized plot, Fig. 3(b), despite the t analysis suggesting opposite magnitudes of t within the two cells. Using Eq. (5), we tried correcting the data based on the t values to obtain hydrostatic a_p lattice parameters and associated volumes. However, the result was to dramatically increase the discrepancy between the two datasets in $P - V$ space rather than improve consistency as expected. The correction additionally increased scatter within the dataset from each DAC. Based on the excellent agreement between the two datasets without correction, we believe the nonhydrostaticity effects were small even without Zr fully encased in Bi. We therefore opted not to include the stress correction and present EoS fits to the uncorrected XRD data.

IV. RESULTS

Although the aim of this study was to investigate the existence of an isostructural transition in β-Zr at 83 GPa, high-precision volume measurements were also made of the α-, ω-, and β-Zr phases below 50 GPa, including measurements of volume changes at the α-ω and ω-β transitions. We also collected decompression data on one sample to measure the zero-pressure lattice parameters and volume of the ω-phase, which is metastable at ambient pressure. From the measured d spacings of seven peaks at ambient pressure, we obtained ω-phase lattice parameters of $a_0 = 5.044(3)$ Å, and $c_0 = 3.137(1)$ Å, giving $V_0 = 23.05(3)$ Å^3/atom, similar

TABLE I. Vinet and AP2 equation of state parameters obtained from fits to the combined β-Zr data from DACs 1, 2, 3, and 4 (as tabulated in Table S8). The Vinet EoS parameters reported in Refs. [8–11] are also given, along with the parameters obtained from a fit of a Vinet EoS to the original β-Zr data of Anzellini *et al.* [10]. The bold values were fixed during the fits.

Reference	EoS	V_0 (Å^3)	K_0 (GPa)	K_0'	Pressure range (GPa)
This study	AP2	**22.6**	87.4(4)	3.51(2)	35–240
This study	AP2	23.0(2)	79(4)	3.65(6)	35–240
This study	Vinet	**22.6**	83.0(5)	3.91(2)	35–240
This study	Vinet	23.7(2)	61(4)	4.41(10)	35–240
Anzellini *et al.* [10] R4	Vinet	**22.6**	93(1)	3.20(9)	35–142
Anzellini original R4	Vinet	**22.6**	83.8(4)	3.82(2)	35–152
O′Bannon *et al.* R1 [11]	Vinet	**22.6**	95.4(3)	3.15(2)	35–80
O′Bannon *et al.* R2 [11]	Vinet	**22.6**	95.1(8)	3.13(4)	35–74
O′Bannon *et al.* R3 [11]	Vinet	**22.6**	91.8(7)	3.25(5)	35–71
Stavrou *et al.* [8]	Vinet	**22.6**	80(5)	3.35(40)	30–57.5
Pigott *et al.* [9]	Vinet	**22.6**	105(1)	2.5(1)	35–50
Combined data[a]	AP2	23.55(11)	69(2)	3.81(4)	35–240
Combined data[a]	Vinet	24.41(15)	51(2)	4.64(6)	35–240

[a]Fits using data from this study, Ref. [11], and the Anzellini R2 and original R4 data we acquired through private communication.

to previous values of 22.76 Å^3/atom and 22.99 Å^3/atom reported by Jamieson [42] and Zhao *et al.* [43], respectively.

The resulting volume compressibility of Zr from 0 to 240 GPa is shown in Fig. 3(a). The data from all five samples are in excellent agreement, and fits to the compressibility data for the α and ω phases give the EoS parameters listed in Table II. The volume changes ($\Delta V/V_0$) at the $\alpha-\omega$ and $\omega-\beta$ transitions are -1.1% and -3.5%, respectively, in excellent agreement with previous determinations. These volumes were evaluated at transition pressures of 11.3 $\pm$ 0.2 and 34.2 $\pm$ 1.4 GPa, respectively. Most importantly, in terms of the principal aim of this study, we see no discontinuity in either the atomic volume or compressibility of β-Zr at 83 GPa.

As said earlier, linearization of compression data accentuates changes in behavior compared to that evident in a simple P-V plot such as Fig. 3(a). Our linearized compression data, shown in the form of a x-η_{APL} plot [see Eq. (2)], are shown in Fig. 3(b). The equivalent quasilogarithmic pressure scale is shown on the top axis in Fig. 3(b). In such a plot, "simple" materials, e.g., Cu or Au, exhibit linear behavior with a positive gradient [in the form of the plot shown in Fig. 3(b)] and are well described by an AP1 EoS, while "regular" materials exhibit slightly nonlinear behavior, indicative of higher-order APL (L $\geqslant$ 2) equations but with *small* values of c_2 [see Eq. (1)]. "Irregular" materials exhibit large deviations from the ideal gradient or strongly nonlinear behavior and require higher-order APL (L $\geqslant$ 2) EoSs with *large* values of c_2 and higher-order terms. Holzapfel [23] draws a distinction between "regular" and "irregular" EoS behavior based on evaluating

$$|c_2 - (c_0 - c_{0,\mathrm{ideal}})|. \tag{12}$$

Values below 0.5 are defined as "regular" where $c_{0,\mathrm{ideal}} = \beta_{\mathrm{ideal}}\sigma_0$, and $\sigma_0 = (3ZV_0/(4\pi))^{1/3}$.

The negative gradient exhibited by the linearized data from α-Zr suggests it is irregular and is more compressible than would be expected from its ambient electron density. Such behavior is typically observed in metals undergoing *s-d* electron transfer, for example [19]. The linearized compressibility for β-Zr displays linear behavior with no evidence of any discontinuity at 83 GPa. However, although the data are linear and have a positive gradient, a single-parameter AP1 EoS provides a very poor fit [see Fig. 3(b)] to β-Zr. Evaluation of Eq. (12) using the best fitted AP2 EoS parameters from Table S2 yields $|c_2 - (c_0 - c_{0,\mathrm{ideal}})| = 2.03$, placing bcc-Zr firmly in the category of an irregular metal, as illustrated in Fig. 3(b). Such a result may indicate the likelihood of additional phase

TABLE II. Vinet and AP2 equation of state parameters obtained from fits to the combined α-Zr and ω-Zr data from DACs 1, 2, 3, 4, and 5 (as tabulated in Tables S6 and S7). The Vinet EoS parameters reported in Refs. [8,10] are also given. The bold values were fixed during the fits.

Reference	EoS	V_0 (Å^3)	K_0 (GPa)	K_0'	Pressure range (GPa)
α-Zr (this study)	Vinet	**23.32**	113.7(7)	**1**	0–11
α-Zr (this study)	AP2	**23.32**	116(2)	0.2(4)	0–11
ω-Zr (this study)	Vinet	**23.05**	98(2)	3.6(2)	0–33
ω-Zr (this study)	AP2	**23.05**	98.6(15)	3.5(2)	0–33
α-Zr Ref. [10]	Vinet	23.29(1)	99.3(12)	2.92(13)	0–22
ω-Zr Ref. [10]	Vinet	23.27(11)	78(7)	4.45(62)	0–36
ω-Zr Refs. [8,10]	Vinet	**23.6**	78(6)	2.95(70)	12–31

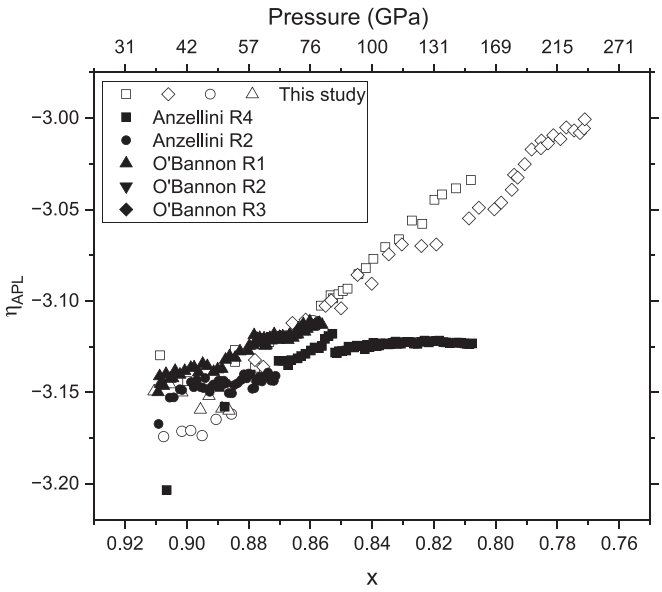


FIG. 5. Enlarged view of the linearized compressibility of β-Zr from all four samples in this study (plotted with unfilled symbols), along with the data from samples R2 and R4 of Anzellini *et al.* [10], and Runs 1–3 of O'Bannon *et al.* [11]. Our data are in excellent agreement with that of O'Bannon *et al.*, but while the data from Anzellini are in good agreement with ours up to 83 GPa, the data clearly diverge above that point.

transformations with increasing pressure which aid to regularize the compressibility behavior [17,44].

The linearized data for only β-Zr are shown in Fig. 5 along with that from Runs 2 and 4 of Anzellini *et al.* [10], and Runs 1–3 of O'Bannon *et al.*; [11]. The slight difference in the *P-V* data obtained from samples DAC1 and DAC2 above 115 GPa, which is not visible in Fig. 3(a), is more visible in the linearized plot. Our data are in excellent agreement with that of O'Bannon *et al.* and also with that of Anzellini *et al.* for $P < 60$ GPa ($x > 0.88$). Between 60 and 80 GPa, the gradient of Anzellini's data is very similar to ours and O'Bannon's, even if it is displaced slightly in η_{APL}. However, above the discontinuity at 83 GPa, Anzellini's published data diverge strongly from our own. Indeed, the linearized data of Anzellini show a gradual reduction in its gradient [more evident in the linearized data shown in Fig. 1(b)] such that it may even become negative at pressures above 170 GPa. Such curvature in linearized plots, leading to nonphysical compressibility, has been reported previously for Vinet equations of state (EoS) extrapolated beyond the range of the fitted data [20].

Figure 5 also illustrates that there is surprisingly little scatter in the linearized R4 data of Anzellini above 83 GPa, and certainly much less than in the R2 and R4 data below that pressure. Indeed, close examination of Fig. 5 of Ref. [10] shows that the Vinet EoS fitted to the data passes directly through the center of *every* observed data point above 83 GPa, while the fit below that pressure, and particularly between 65 and 83 GPa, is much poorer. The exceptional agreement between the data collected above 83 GPa and the Vinet EoS is most evident in Fig. 1(b), which shows both the linearized data and linearized EoS. Even in the linearized data, where differences are greatly

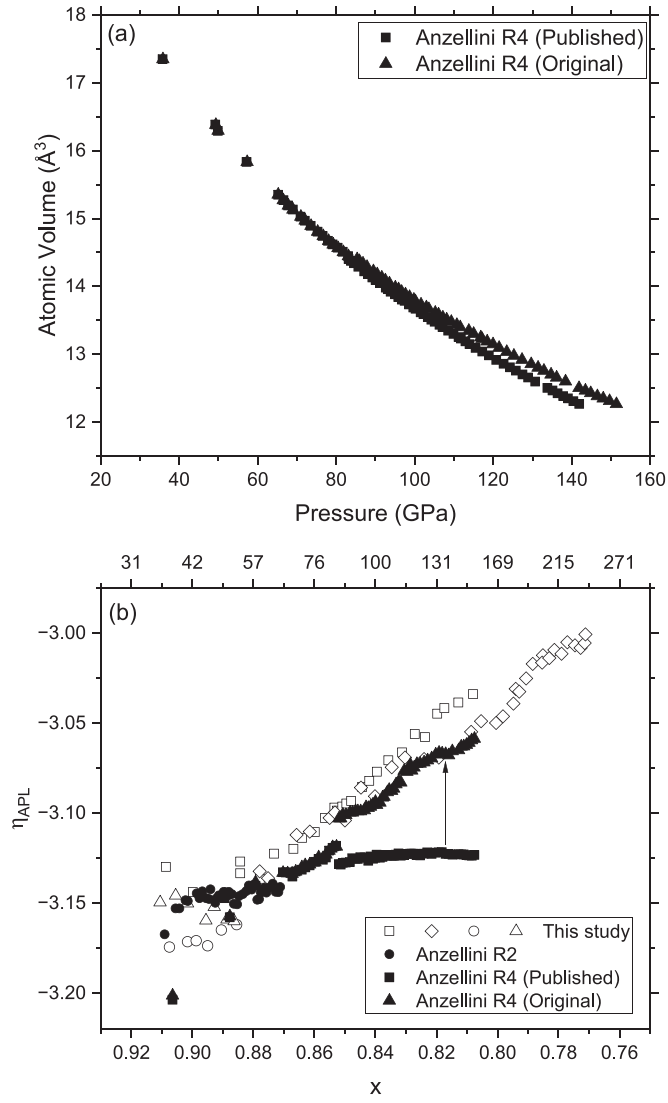


FIG. 6. (a) The compressibility and (b) linearized compressibility of β-Zr from the published R4 data of Anzellini (■), and from the original R4 data (▲) sent by the authors. The original data are in excellent agreement with the published data up to 83 GPa, above which the two diverge. Rather than the small volume decrease at 83 GPa seen in the published data, as highlighted previously in Fig. 1(a), the original data show a small nonphysical volume *increase* at the same pressure, observable as a discontinuity in the linearized data. However, above 83 GPa, the compressibility of the original data is in excellent agreement with that from the present study, the data from which are plotted with unfilled symbols in Fig. 6(b). The arrow highlights the displacement of the published data.

amplified, the EoS and data show excellent agreement above 83 GPa. Indeed, the agreement between the observed data and the fitted EoS is so good that it suggests that the data above 83 GPa may have used pressures *calculated* from the Vinet EoS, rather than the experimentally observed pressures.

We contacted the authors of Ref. [10] and inquired whether this might be possible. They sent the original data from their study, and the *P-V* and linearized data are shown in Figs. 6(a) and 6(b), respectively, along with the as-published data. We have also included the two datasets in Table S5 for

completeness. It is clear that while the atomic volume values are the same in both sets of data, the pressures above 83 GPa in [10] are not those of the original data, which are 2–9 GPa higher. Using the original data provided by the authors of [10] results in (i) a small $\Delta V/V$ *increase* of 0.4% at 83 GPa rather than a decrease of 0.2%, and (ii) *much* better agreement with our own data above 83 GPa. Indeed, the original data of Anzellini *et al.* are indistinguishable from our own above 83 GPa, even after linearization, which would greatly amplify any differences between the data sets.

Using the volumes of the pressure calibrant provided by the previous authors, and the Vinet EoS they reported ($V_0 = 22.6\,\text{Å}^3/\text{atom}$, $K_0 = 93$ GPa, and $K_0' = 3.2$), we confirmed that the pressures above 83 GPa in [10] are those calculated from this Vinet EoS, thereby explaining the excellent agreement between the two. The reasons why such data were used only above 83 GPa are unknown, as is the origin of the Vinet EoS parameters reported in [10], as we were unable to obtain them from fits to the original data. *Note added:* During the review process for this manuscript, an erratum was released [45] for the experimental data reported in [10] which presents their corrected data and identifies the anomaly reported in this work. The corrected data points are identical to those included in Table S5.

Refinements of AP2 and Vinet equations of state to the combined β-Zr data from all four of our samples gave excellent fits [see Fig. 3(a)], and the resulting parameters are listed in Table 1. EoS fits with V_0 constrained to be 22.6 $\text{Å}^3/\text{atom}$ (as used in [9–11]) resulted in a systematic misfit to our data in the 35–55 GPa pressure range, however we have included the parameters for comparison. We therefore also performed fits with V_0 unconstrained. The resulting fits had very high correlations between the parameters, and gave very different values of V_0 and K_0 (see Table I). However, the fits to our data were clearly improved with a variable V_0. It is not clear to us where the constrained value of $V_0 = 22.6\,\text{Å}^3/\text{atom}$ originated from as it appears without comment and has been reproduced from study to study. We note that since β-Zr is not stable at ambient conditions, the parameter V_0 has no real physical significance and is simply acting as a fitting parameter.

Also given in Table I are the parameters from the Vinet fits to β-Zr reported in Refs. [8–11]. We have also fitted the original data of Anzellini *et al.* with a Vinet EoS, and the parameters are listed in Table 1. Comparing the parameters from the Vinet fits shows that those obtained from the current data (with $V_0 = 22.6$ $\text{Å}^3/\text{atom}$) are in excellent agreement with those obtained from refitting the original data of Ref. [10], while the other reported fits typically have a larger K_0 and a smaller K_0'. However, these other data were collected over a much smaller pressure range (typically only 35–80 GPa), from which it is more difficult to determine the values of the highly correlated K_0 and K_0' at 0 GPa, a pressure at which there is no data on β-Zr.

The volume differences between the Vinet EoS fit to our data (with V_0 unconstrained) and previous experimental and computational results are shown in Figs. 7(a) and 7(b), respectively.While the deviations of the experimental data of Stavrou [8], Pigott [9], as-published Anzellini [10], and Liu [16] are substantial, the experimental data of O'Bannon [11], and the DFT-derived equations of state of Wang [46], Stavrou [8], Anzellini [10], O'Bannon [11], and Ning [47], are in very much better agreement with our own data. For completeness, Table I also includes the parameters resulting from a fit to the combined β-Zr datasets of O'Bannon *et al.* [11], Anzellini *et al.*'s [10] original data, and our own study.

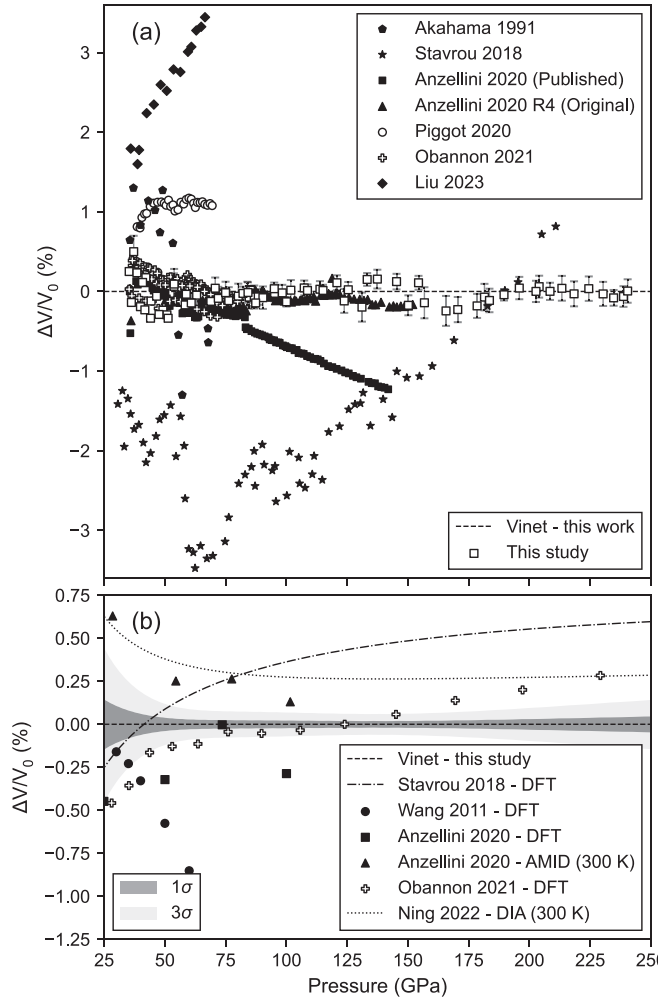


FIG. 7. The percentage volume differences ($\Delta V/V_0$), as a function of pressure, between the Vinet EoS fit to our data (with V_0 unconstrained) and previous (a) experimental and (b) computation data from 25 to 250 GPa. The central horizontal dashed line in each plot gives the Vinet fit from the present study using the parameters from Table I. Data are from sources [7–11,16,46,47]. The shaded gray region corresponds to 1σ and 3σ confidence intervals of our Vinet fit. Data from (a) over the reduced pressure ranges 40–75 and 70–96 GPa are also given in Fig. S6 of the Supplemental Material [24].

While the equations of state of the α and ω phases were not the main focus of this study, we have fitted the data from both phases shown in Fig. 3(a). For α-Zr, we constrained $V_0 = 23.315$ $\text{Å}^3/\text{atom}$, our measured value at ambient pressure. This is comparable to the literature value of 23.279 $\text{Å}^3/\text{atom}$ given in Ref. [48]. In order to overcome the issue of highly correlated parameters described above, and knowing that ω-Zr is metastable at ambient pressure, we measured V_0 for ω-Zr by slowly decreasing the pressure on DAC3 to ambient obtaining a $V_0 = 23.05(3)$ $\text{Å}^3/\text{atom}$.

V. DISCUSSION AND CONCLUSIONS

We have measured the compression curves of the α, ω, and β phases of Zr to 240 GPa at 300 K in aluminium and bismuth pressure media. It is clear from the linearized data plotted in Figs. 4 and 5(b) that there is no change in either the atomic volume or compressibility of β-Zr at 83 GPa within the resolution of the present experiments. The previous discontinuities present in the published data of Anzellini *et al.* arose from the use of calculated pressures above 83 GPa rather than the experimentally observed pressures. Although a small (nonphysical) volume increase is present in these data at 83 GPa, the compressibility of the original data above that pressure is in almost perfect agreement with our own. Our compressibility data are also in excellent agreement with the DFT-derived equations of state for β-Zr [7–11,16,46,47], with maximum atomic volume discrepancies of only $\sim$0.5% ($\Delta V/V_0$) at 225 GPa [Fig. 7(b)]. Thus, our compression study on β-Zr aligns with the findings of previous works [9–13] with data showing a smooth volume compression and an absence of an isostructural phase transition in the pressure range 56–83 GPa within the resolution of the present experiments. Our work extends this result and provides an accurate Zr-EoS up to the maximum pressure achieved of 240 GPa.

ACKNOWLEDGMENTS

British Crown Owned Copyright 2026/AWE. Published with permission of the Controller of His Britannic Majesty's Stationery Office. This work was supported by Grants No. EP/R02927X/1 and No. EP/Z533671/1 from the UK Engineering and Physical Sciences Research Council (EPSRC). C.M.L. and C.R.R. are grateful to S.G. MacLeod and AWE for the award of their studentships (No. WT13356629 and No. WT14175294). We acknowledge DESY (Hamburg, Germany), a member of the Helmholtz Association HGF, for the provision of experimental facilities. Parts of this research were carried out at PETRA III and we would like to thank N. Giordano and H.-P. Liermann for their assistance in using beamline P02.2. Beamtime was allocated for Proposals No. I-20240226 and No. I-20240993 EC. We would also like to thank Agnès Dewaele for providing the original R4 β-Zr data from Ref. [10].

J.D.M., C.V.S., C.M.L., and M.I.M. conceptualized the experiments. All authors performed the experiments. J.D.M. and M.I.M. supervised, performed the formal analysis, visualization and wrote the original draft. All authors reviewed and edited the manuscript. M.I.M. secured funding and resources.

The authors have no conflicts to disclose.

DATA AVAILABILITY

The data that support this article are available from the corresponding authors upon reasonable request.

[1] B. S. Hickman, The formation of omega phase in titanium and zirconium alloys: A review, J. Mater. Sci. **4**, 554 (1969).

[2] J. Ballor, T. Li, F. Prima, C. J. Boehlert, and A. Devaraj, A review of the metastable omega phase in beta titanium alloys: The phase transformation mechanisms and its effect on mechanical properties, Int. Mater. Rev. **68**, 26 (2023).

[3] N. Velisavljevic, S. MacLeod, and H. Cy, Titanium alloys at extreme pressure conditions, in *Titanium Alloys - Towards Achieving Enhanced Properties for Diversified Applications* (InTech, 2012).

[4] S. Sikka, Y. Vohra, and R. Chidambaram, Omega phase in materials, Prog. Mater. Sci. **27**, 245 (1982).

[5] Y. Akahama, S. Kawaguchi, N. Hirao, and Y. Ohishi, Observation of high-pressure bcc phase of titanium at 243 GPa, J. Appl. Phys. **128**, 035901 (2020).

[6] H. Xia, S. J. Duclos, A. L. Ruoff, and Y. K. Vohra, New high-pressure phase transition in zirconium metal, Phys. Rev. Lett. **64**, 204 (1990).

[7] Y. Akahama, M. Kobayashi, and H. Kawamura, High-pressure X-ray diffraction study on electronic $s-d$ transition in zirconium, J. Phys. Soc. Jpn. **60**, 3211 (1991).

[8] E. Stavrou, L. H. Yang, P. Söderlind, D. Aberg, H. B. Radousky, M. R. Armstrong, J. L. Belof, M. Kunz, E. Greenberg, V. B. Prakapenka, and D. A. Young, Anharmonicity-induced first-order isostructural phase transition of zirconium under pressure, Phys. Rev. B **98**, 220101(R) (2018).

[9] J. S. Pigott, N. Velisavljevic, E. K. Moss, D. Popov, C. Park, J. A. Van Orman, N. Draganic, Y. K. Vohra, and B. T. Sturtevant, Room-temperature compression and equation of state of body-centered cubic zirconium, J. Phys.: Condens. Matter **32**, 12LT02 (2020).

[10] S. Anzellini, F. Bottin, J. Bouchet, and A. Dewaele, Phase transitions and equation of state of zirconium under high pressure, Phys. Rev. B **102**, 184105 (2020).

[11] E. F. O'Bannon, P. Söderlind, D. Sneed, M. J. Lipp, H. Cynn, J. S. Smith, C. Park, and Z. Jenei, High pressure stability of β-Zr: No evidence for isostructural phase transitions, High Press. Res. **41**, 247 (2021).

[12] G. Jyoti and S. C. Gupta, Theoretical analysis of the isostructural transition in Zr at 53 GPa, J. Phys.: Condens. Matter **6**, 10273 (1994).

[13] C. W. Greeff, Phase changes and the equation of state of Zr, Modell. Simul. Mater. Sci. Eng. **13**, 1015 (2005).

[14] A. W. Lawson and T.-Y. Tang, Concerning the high pressure allotropic modification of cerium, Phys. Rev. **76**, 301 (1949).

[15] I.-K. Jeong, T. W. Darling, M. J. Graf, T. Proffen, R. H. Heffner, Y. Lee, T. Vogt, and J. D. Jorgensen, Role of the lattice in the $\gamma \rightarrow \alpha$ phase transition of Ce: A high-pressure neutron and x-ray diffraction study, Phys. Rev. Lett. **92**, 105702 (2004).

[16] L. Liu, Q. Jing, H. Y. Geng, Y. Li, Y. Zhang, J. Li, S. Li, X. Chen, J. Gao, and Q. Wu, Revisiting the high-pressure behaviors of zirconium: Nonhydrostaticity promoting the phase transitions and absence of the isostructural phase transition in β-zirconium, Materials **16**, 5157 (2023).

[17] C. V. Storm, J. D. McHardy, S. E. Finnegan, E. J. Pace, M. G. Stevenson, M. J. Duff, S. G. MacLeod, and M. I. McMahon, Behavior of rubidium at over eightfold static compression, Phys. Rev. B **103**, 224103 (2021).

[18] C. V. Storm, G. A. Woolman, C. M. Lonsdale, J. D. McHardy, M. J. Duff, G. J. Ackland, and M. I. McMahon, Experimental and computational study of the core-level crossing transition in iridium at high pressure, Phys. Rev. B **109**, 024101 (2024).
[19] W. B. Holzapfel, Physics of solids under strong compression, Rep. Prog. Phys. **59**, 29 (1996).
[20] W. B. Holzapfel, Equations of state for solids under strong compression, High Press. Res. **16**, 81 (1998).
[21] PlotDigitizer: Version 4.5 (2024).
[22] W. B. Holzapfel, Equations of state for ideal and real solids under strong compression, Europhys. Lett. **16**, 67 (1991).
[23] W. B. Holzapfel, Equations of state for solids under strong compression, Z. Kristallogr. **216**, 473 (2001).
[24] See Supplemental Material at http://link.aps.org/supplemental/10.1103/zp3m-kjpc for additional figures, data tables, EOS parameters, and strength analysis examples.
[25] R. Boehler, New diamond cell for single-crystal x-ray diffraction, Rev. Sci. Instrum. **77**, 115103 (2006).
[26] R. Boehler and K. De Hantsetters, New anvil designs in diamond-cells, High Press. Res. **24**, 391 (2004).
[27] C. V. Storm, J. D. McHardy, M. J. Duff, S. G. MacLeod, E. F. O'Bannon, and M. I. McMahon, The stress state in bismuth to 298 GPa and its use as a pressure transmitting medium and pressure marker at multi-megabar pressures, J. Appl. Phys. **133**, 245904 (2023).
[28] Y. Akahama, M. Nishimura, K. Kinoshita, H. Kawamura, and Y. Ohishi, Evidence of a fcc-hcp transition in aluminum at multimegabar pressure, Phys. Rev. Lett. **96**, 045505 (2006).
[29] K. Glazyrin, S. Khandarkhaeva, T. Fedotenko, W. Dong, D. Laniel, F. Seiboth, A. Schropp, J. Garrevoet, D. Brückner, G. Falkenberg, A. Kubec, C. David, M. Wendt, S. Wenz, L. Dubrovinsky, N. Dubrovinskaia, and H.-P. Liermann, Submicrometer focusing setup for high-pressure crystallography at the Extreme Conditions beamline at PETRAIII, J. Synchrotron Radiat. **29**, 654 (2022).
[30] C. Prescher and V. B. Prakapenka, Dioptas: A program for reduction of two-dimensional X-ray diffraction data and data exploration, High Press. Res. **35**, 223 (2015).
[31] V. Petricek and M. Dusek, *The Crystallographic Computing System JANA2000* (Institute of Physics, Praha, Czech Republic, 2000).
[32] T. J. B. Holland and S. A. T. Redfern, Unit cell refinement from powder diffraction data: The use of regression diagnostics, Mineral. Mag. **61**, 65 (1997).
[33] A. Dewaele, P. Loubeyre, and M. Mezouar, Equations of state of six metals above 94 GPa, Phys. Rev. B **70**, 094112 (2004).
[34] A. K. Singh, The lattice strains in a specimen (cubic system) compressed nonhydrostatically in an opposed anvil device, J. Appl. Phys. **73**, 4278 (1993).
[35] A. K. Singh and T. Kenichi, Measurement and analysis of nonhydrostatic lattice strain component in niobium to 145 GPa under various fluid pressure-transmitting media, J. Appl. Phys. **90**, 3269 (2001).
[36] A. K. Singh, Analysis of nonhydrostatic high-pressure diffraction data (cubic system): Assessment of various assumptions in the theory, J. Appl. Phys. **106**, 043514 (2009).
[37] A. K. Singh, H. K. Mao, J. F. Shu, and R. J. Hemley, Estimation of single-crystal elastic moduli from polycrystalline X-ray diffraction at high pressure: Application to FeO and iron, Phys. Rev. Lett. **80**, 2157 (1998).
[38] A. K. Singh, C. Balasingh, H.-K. Mao, R. J. Hemley, and J. Shu, Analysis of lattice strains measured under nonhydrostatic pressure, J. Appl. Phys. **83**, 7567 (1998).
[39] A. Singh, E. Menendez-Proupin, G. Gutierrez, Y. Akahama, and H. Kawamura, Nonhydrostatic compression of bismuth to 222GPa: Some constraints on elasticity of the bcc-phase, J. Phys. Chem. Solids **67**, 2192 (2006).
[40] A. K. Singh and K. Takemura, Negative differential stresses in niobium: Analysis of x-ray measured pressure-volume data, J. Appl. Phys. **128**, 075901 (2020).
[41] C. M. Lonsdale, J. D. McHardy, C. V. Storm, K. Glazyrin, M. Mezouar, and M. I. McMahon, A closer look under extreme pressure: Sub-micron diffraction mapping in a diamond anvil cell, High Press. Res. **46**, 56 (2026).
[42] J. C. Jamieson, Crystal structures at high pressures of metallic modifications of compounds of indium, gallium, and aluminum, Science **139**, 845 (1963).
[43] Y. Zhao, J. Zhang, C. Pantea, J. Qian, L. L. Daemen, P. A. Rigg, R. S. Hixson, G. T. Gray, Y. Yang, L. Wang, Y. Wang, and T. Uchida, Thermal equations of state of the α, β, and ω phases of zirconium, Phys. Rev. B **71**, 184119 (2005).
[44] C. V. Storm, S. E. Finnegan, J. D. McHardy, M. J. Duff, M. I. McMahon, S. G. MacLeod, E. Plekhanov, and C. Weber, Unified high-pressure phase-transition sequence in the f-electron metals: $oF16 \rightarrow oF8$ transition in terbium, Phys. Rev. Lett. **135**, 136101 (2025).
[45] S. Anzellini, F. Bottin, J. Bouchet, and A. Dewaele, Erratum: Phase transitions and equation of state of zirconium under high pressure [Phys. Rev. B 102, 184105 (2020)], Phys. Rev. B **113**, 179901 (2026).
[46] B.-T. Wang, P. Zhang, H.-Y. Liu, W.-D. Li, and P. Zhang, First-principles calculations of phase transition, elastic modulus, and superconductivity under pressure for zirconium, J. Appl. Phys. **109**, 063514 (2011).
[47] B.-Y. Ning, Pressure-induced structural phase transitions of zirconium: An *ab initio* study based on statistical ensemble theory, J. Phys.: Condens. Matter **34**, 505402 (2022).
[48] J. Donohue, *The Structures of the Elements* (J. Wiley & Sons, London, 1974).